International Journal of Marine Energy 14 (2016) 161–179

Contents lists available at ScienceDirect

International Journal of Marine Energy

journal homepage: www.elsevier.com/locate/ijome

Wave–current interaction effects on tidal stream turbine performance and loading characteristics

S.C. Tatum, C.H. Frost, M. Allmark, D.M. O'Doherty, A. Mason-Jones, P.W. Prickett, R.I. Grosvenor, C.B. Byrne, T. O'Doherty *

School of Engineering, Cardiff University, Queen's Buildings, The Parade, Cardiff CF24 3AA, United Kingdom

ARTICLE INFO

Article history:
Received 13 March 2015
Revised 26 August 2015
Accepted 7 September 2015
Available online 30 September 2015

Keywords:
Tidal turbines
Computational modelling
Fluid structural interaction

ABSTRACT

The transient interaction between tidal currents and the rotation of a horizontal axis turbine rotor have the potential to induce high asymmetric loadings, which are subsequently transmitted to the drive shaft and potentially high speed drive train components. To mitigate the potential for early component failure, analysis of asymmetric loading on marine turbines is fundamental to the design process. To investigate these loads a turbine mounted on a circular stanchion has been used to highlight the effects of introducing more realistic boundary conditions. Depending on their wavelength, waves can also have a significant effect on the overall design decisions and placement of devices. Thrust loading and bending moments applied to the drive shaft can be of the order of hundreds of kN and kN m respectively.

Knowledge of the flow regime can allow designers to evaluate material selection for components and incorporate some deformation capability of the turbine blades to increase the power output and potentially alleviate some of the stress distribution through key structural points. The resulting data can then be used to estimate component life via fatigue prediction.

This paper includes a multi-physics approach to modelling tidal energy devices and the potential for modelling to inform device condition monitoring.

* Corresponding author. Tel.: +44 029 2087 5366.
E-mail addresses: tatumsc@cardiff.ac.uk (S.C. Tatum), frostc1@cardiff.ac.uk (C.H. Frost), odohertydm@cardiff.ac.uk (D.M. O'Doherty), mason-jonesa@cardiff.ac.uk (A. Mason-Jones), prickett@cardiff.ac.uk (P.W. Prickett), grosvenor@cardiff.ac.uk (R.I. Grosvenor), byrne@cardiff.ac.uk (C.B. Byrne), odoherty@cardiff.ac.uk (T. O'Doherty).

http://dx.doi.org/10.1016/j.ijome.2015.09.002
2214-1669/

Nomenclature

Cp	power coefficient (−)
Ct	thrust coefficient (−)
L	wavelength (m)
k	wavenumber (m^{-1})
H	wave height (m)
λ	tip speed ratio (−)
ω	angular velocity of wave (rad s^{-1})
g	gravity (m s^{-2})
T	wave period (s)
h	water depth (m)

1. Introduction

The EU has targeted renewable energy to provide 20% of the total energy mix by 2020 [1] in comparison the UK target is 15% of the UK energy demands from renewable sources by 2020 [2]. In order to meet and sustain the targets set by 2020 and beyond, the UK and EU at large must continue to address the imbalance in the renewable energy mix. The potential for sustainable production through wave and tidal energy conversion has resulted in large investment from industry and governments. A practical and economical resource of tidal current and wave energy resource of 70 TWh/year around the UK shores has been identified, which would contribute to 20% of UK's total industrial, commerce and domestic electricity demands [3].

The long term predictability of tides is the main advantage of tidal power over other renewable energy sources since it allows any phase change in power productions between wind and or other tidal stream and wave sites to be balanced. The two leading techniques in energy conversion for tidal range power generation are impoundment schemes such as a barrage or tidal lagoon and tidal stream turbines (TSTs). The impoundment schemes offer large scale solutions, as documented in the La Rance Tidal Power Plant run by EDF Energy which produces 0.54 TWh/year [4], whilst TSTs offer bespoke solutions to fit the local environment and since they are submerged, they are less intrusive than impoundment schemes and minimise the impact on the marine and costal environment.

The introduction of TSTs into the UK energy mix can only be a positive step since the UK has some of the strongest currents in the world, with a number of areas identified as viable sites for installing tidal energy devices [3]. Ideal conditions for tidal stream turbines are; a free stream velocity of 2–3 m/s and a depth of 20–30 m, at least for early stage implementation with deeper water designs (>40 m) introduced as the industry matures. Current developments include the DeltaStream device which is being installed in the Ramsey Sound, Pembrokeshire [5], and the array, of SeaGen S turbines, in the Skerries site off Anglesey [6]. The success of these initiatives is dependent on a thorough understanding of the hydrodynamic forces applied to the TST, its scale, blade design and experiential knowledge acquired from environmental monitoring, which for example has led to actively pitch controlling the blades to limit the maximum rotational speed of the rotors to 14 rpm [7]. The hydrodynamic forces cause considerable loading on the blades, resulting in blade deformation. The magnitude of the deformation will be dependent on the design of the blades, their internal structure and materials used. However, the combined loading on the blades and hub of the rotor is transmitted to the drive shaft, and knowledge of these resultant transient forces is essential for developers to optimise the success of their design.

The simplest scenario for determining the hydrodynamic forces is to consider the effects of a uniform tidal current. However, in reality, the current is typified by a high shear in the velocity profile through the water column, turbulence and surface waves and these all need to be considered in determining the loads on a TST. Work on the effects of highly shearing profiles and levels of turbulence have

been considered by Mason-Jones et al. (2008) [8] and Morris (2014) [9]. Wave effects are likely to be critical as they are known to penetrate the water column to a depth of approximately 50% of their wavelength [10]. This can be further complicated by the fact that the direction of the wave does not necessarily align itself to the direction of the current as shown by Lewis et al. (2014) [11].

Myers and Bahaj [12] provided a clear indication, shown in Fig. 1, of the primary flow characteristics of the tidal current. The scale of the variations in the bathymetry has a significant effect of the shape of the flow profile through the water column. The greater the drag effects, the potentially greater the velocity shear. Sea surface gravity waves result in an oscillatory motion under the water surface. If particles are considered to be suspended through the water column, they would move in an orbital fashion with the magnitude of the oscillations diminishing with distance from the water surface, with motion ceasing at a depth of approximately half the wavelength of the wave. Once a tidal current is superimposed upon the wave, the orbital motion is stretched, yielding an elliptical particle trajectory. This effect is also increased as the water depth decreases in relation to the wave amplitude.

A 2010 study carried out by Galloway et al. [13] examined to effect of 0.08 m high waves with a time period of 1.43 s on a scaled model turbine with swept area 0.5 m^2 in a towing tank. The aim of the study was to quantify the effect of the complex circular motion caused by the waves on a turbine, in order that devices could be placed higher in the water column where the tidal flow is faster, even though the wave effect would be stronger. The device was towed at 1.5 m/s, which at the high Reynolds number can be safely scaled to a 16 m diameter device at 4 m/s. They found that the waves had no effect on the average performance characteristics of thrust and power, due to the fact that the motion of the waves moves back and forth, effectively cancelling out and leaving the average unchanged. However, the cyclic effect was found to be significant, with variations of 37% of the mean for thrust, and 35% of the mean for power. The proposed effects of this are increased fatigue and the requirement for more complex power conditioning.

This was confirmed by a similar scale model towing tank experimental study by Lust et al. [14], in which they found the average power and thrust remained unchanged by the wave climate. However, they also found that the large cyclic variations yielded poor power quality and predicted a requirement for turbine materials with much greater fatigue resistance due to varying thrust. Large variations in performance parameter as well as rotational speed with passing waves were detected, and they determined that varying the turbine height significantly affected the average output power. They concluded that the balance between increasing distance from the passing wave and an increased flow speed near the water surface was crucial for improving performance and maintaining fatigue life. Average performance values were also found to be unchanged in another towing tank experiment by Luznik et al. [15], where the test waves could be scaled up to represent a 90 m wavelength wave with a large wave period of 8 s. They found that the waves caused variations in the average power coefficient, which was 0.38, from a minimum of 0.25 to maximum of 0.45, which is equivalent to a variation of 34% and 18% respectively.

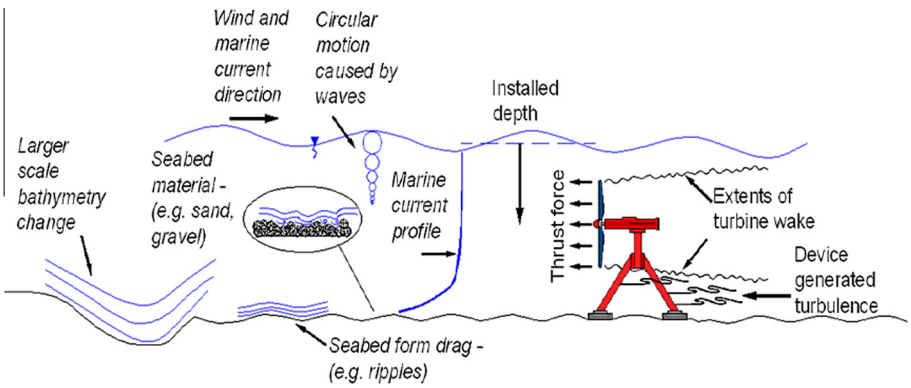

Fig. 1. Variables affecting the flow field around tidal turbines [12].

The aim of this work was therefore to investigate, by the means of numerical modelling, the effects of surface waves on the performance characteristics of a tidal turbine. The approach taken started with steady state uncoupled CFD modelling of the turbine through a range of tip speed ratios (λ) for constant current flow (the uncoupled CFD model), followed by a fully coupled 2-way transient FSI model at peak power for the same current flow (the FSI model). Finally a transient uncoupled CFD model was modelled at peak power for the same current flow, with waves in the same direction as the current (the VOF model). In all cases, the study focussed on the cyclic blade loading from axial thrust loads.

2. Fluid structural interaction modelling (FSI)

Previous FSI studies of marine turbines include a loosely coupled approach, via a surface panel code to link the CFD to the FEA [16]. This work gives a valid insight to the effects of FSI and its consequences on cavitation, power attenuation and stresses on the structure. Whilst it is stated by Nicholls-Lee et al. (2014) [16] that the panel method performs well for undeviating flows, it becomes necessary to model greater details in the hydrodynamic flow field, by using the Reynolds Averaged Navier–Stokes (RANS), Detached Eddy Simulation (DES) or Large Eddy Simulation (LES) models to accurately capture the hydrodynamics. Moreover, with knowledge of the hydrodynamics under extreme conditions it becomes necessary to consider the strong coupling effects between the fluid and the structure. These issues were addressed using a fully coupled 2-way FSI model using a symmetry boundary and single blade by Park et al. (2013) [17]. From the results it was suggested that although the deflection of the blade was relatively small in their study, it was still necessary to consider blade deformation due to a 1.7% drop in maximum power extraction. Morris (20104) [9] established the performance characteristics of a tidal stream whilst allowing for blade deformation a series of quasi-static coupled 2-way FSI models constructed with a homogenous blade material, each subjected to a uniform flow inlet boundary condition. The kinetic energy extraction and its sensitivity to structural stiffness attenuation were investigated by incrementally reducing the materials Young's modulus and noting its effect on the rotor's performance.

2.1. Geometry specifications

The 10 m diameter, 3 bladed steel TST discussed in this paper, utilised a Wortmann FX 63-137 profile, with a 33° twist from the blade root to tip. The blade pitch angle was set to the optimum of 6°. The turbine support structure used was of a simple cylindrical design, based on the work of Mason-Jones et al. (2012) [18] and consisted of a 2.4 m diameter stanchion as shown in Fig. 2. Based on the work of

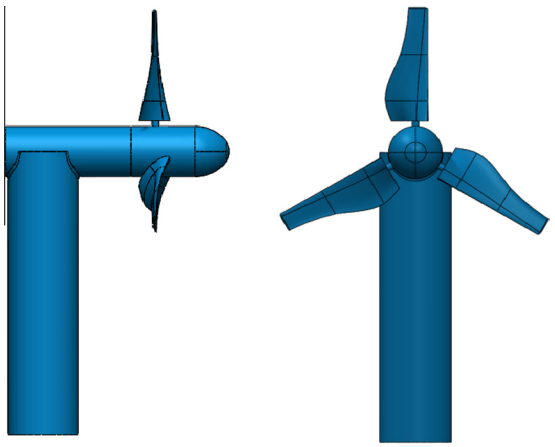

Fig. 2. Side and front view of turbine-stanchion arrangement for all the models.

Frost et al. (2014) [19], the turbine rotor was positioned with a clearance of ~2 m from the stanchion and was orientated to be aligned to the tidal flow.

3. Modelling approach

3.1. The uncoupled CFD model

The uncoupled CFD model consisted of a rectangular domain, 350 m long × 50 m wide × 35 m deep. The turbine was located 100 m downstream from the inlet boundary such that its rotational axis was set at 25 m below the water surface. An axially aligned cylindrical domain was subtracted from the rectangular domain to form a rotational interface domain with a non-conformal interface between the sea and turbine volumes to model the rotation of the turbine. The blade surface interfaces were modelled using tetrahedral elements with face sizing of 0.01 m for the top third and 0.02 m for the bottom two thirds, leading to the root. The rotational interface domain was set with an internal body size of 0.2 m the same value was applied to the external faces of it. In total the water domain had 3.5 million elements with 2 million concentrated about the rotational interface and turbine surfaces. The uncoupled CFD models and coarser meshes than those used in this study have been previously validated using a recirculating water flume and an uncoupled CFD model [19–21].

Inlet boundary conditions were defined as a simple uniform flow of 3.086 m/s (6 knots). The outlet was a pressure outlet, set to atmospheric pressure. All walls of the domain were set to free slip, apart from the seabed which was set to a 'no slip' wall boundary.

For this and subsequent CFD models, the Reynolds Averaged Navier–Stokes equations were applied to relate the Reynolds Stresses to the mean velocity gradients. To close the equations the Shear Stress Transport (SST) was used as the turbulence model. Previous work has used the Reynolds Stress Model; however the simpler and faster SST was used due to the increased model complexity and computational expense of FSI and free surface modelling. The SST model was also found to have a turbulence dissipation rate more suited to this work, yielding better estimations of predicted wake lengths [9]. It also has excellent capabilities for predicting separated flow, yet is advantageous as the scale of the modelling in this paper does not require complete resolution of the boundary layer, yielding an accurate yet faster solution.

3.2. The FSI model

The FSI model utilised the same domain definition as the uncoupled CFD model for the CFD analysis whilst the mesh for the FEA analysis had the same face sizing on the blade surface interfaces and hub interface as the CFD model in order to limit mesh mapping errors for the transfer of data. The face and body cells of the rotating domain in which the turbine was located were sized at 0.2 m, and the support structure cells were 0.1 m on the faces and 0.05 m along the edge. The body of the sea domain was meshed with a coarse element size of 10 m. Hence the final mesh yielded ~1.2 million cells in the sea domain and ~2.4 million cells in the turbine domain. The interface boundaries for the data transfer were set to receive the total mesh displacement from the FEA model and send the total force back from the CFD model.

The setup of the boundary conditions for both the FEA and CFD was done sequentially beginning with the FEA model which was set to match the requirements of the CFD model. That is, a tip speed ratio λ of 3.64, which corresponds to a rotational velocity of 2.25 rad/s. This is the angular velocity at which peak power is extracted for this turbine configuration. (To ensure that the blade tip deflection occurred gradually, allowing the mesh to 'adjust' to the new geometry, the angular velocity was ramped up to the required value). The fluid structural interfaces were then specified, with each blade separated into two faces, front and back. The labelling of these faces is significant as they are required to set the data transfer from the CFD to the FEA and vice versa. The foot of the stanchion was fixed to the floor, using a fixed support. It was assumed for this case that there is no movement of the foundation and the entire bottom face of the stanchion would remain in contact with the seabed. Although not discussed in this paper, it is worth noting that the FEA model also had a number of

outputs including the total deformation, equivalent stress (Von-Mises), equivalent elastic strain, fatigue life and biaxiality, etc. to provide the hydrodynamic effects on the structure.

Once both the CFD and FEA models were setup they were linked/coupled, thus enabling data transfer between the two models. Coupling was set to suit the CFD model with appropriate time steps for the total time equivalent to approximately 6 full turbine rotations. The 6 rotations of the turbine were required to ensure the transient models had 'settled'.

3.3. The VOF model

The VOF model was based on the same definition as the uncoupled CFD model for the water domain, but an additional air domain 350 m long $\times$ 50 m wide $\times$ 15 m deep was added on top of the water domain to allow for a Volume of Fluid (VOF) based analysis. The body of the sea domain was again meshed with a coarse element size of 10 m. An additional, more refined inflation, region was added at the location of the free surface and through a thickness of 8 m to account for the wave chosen in this study, which is discussed in the next section. The turbine was again meshed with a much finer face element size of 0.01 m at the tip, increasing to 0.02 m at the root and hub. The face and body cells of the rotating domain in which the turbine was located were also sized at 0.2 m, with the support structure cells of 0.1 m on the faces and 0.05 m along the edge. As can be seen in Fig. 3 an air domain was added above the 35 m deep sea domain, extending 15 m with 71,893 cells. An inflation layer was applied to the top surface of the water and the bottom surface of the air domain, extending 40 layers into the mesh to allow a much more densely packed mesh in that region. This yielded a final mesh size of $\sim$3.6 million cells in the sea and turbine domains, as with the previously described FSI model and a total mesh size of $\sim$3.65 million cells.

Wave modelling in this study was based around linear wave theory, and sea wave characterisation was carried out with real data, shown in Fig. 4, from the British Oceanographic Database [22] in order to determine the parameters for a realistic, but extreme case, sea wave that might be expected to occur. This was carried out by analysing the significant periods and wave heights of various waves measured at multiple locations around the Welsh and West coasts. A wave was selected based on this data to represent an extreme but plausible case, with a wavelength of 30 m to allow sufficient wave penetration to the turbine [10], and a wave height of 6 m. With this characteristic, the corresponding wave period calculated with linear wave theory [10] was 4.38 s, which is shown on Fig. 4 with the turbine symbol. When this wave was analysed by non-dimensionalising the wave height H and water depth h with gravitational constant g and the wave time period T, and comparing the results to the graph shown in Fig. 5 [23] it was found that the waves fall well outside of the linear regime, due to

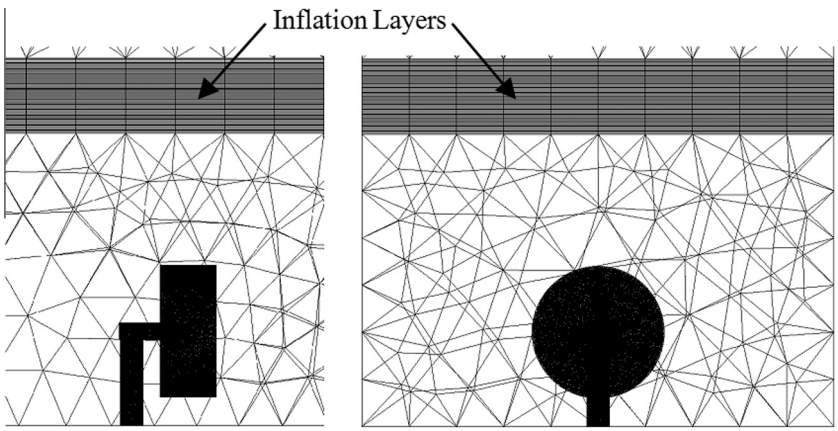

Fig. 3. Meshing arrangement for the VOF.

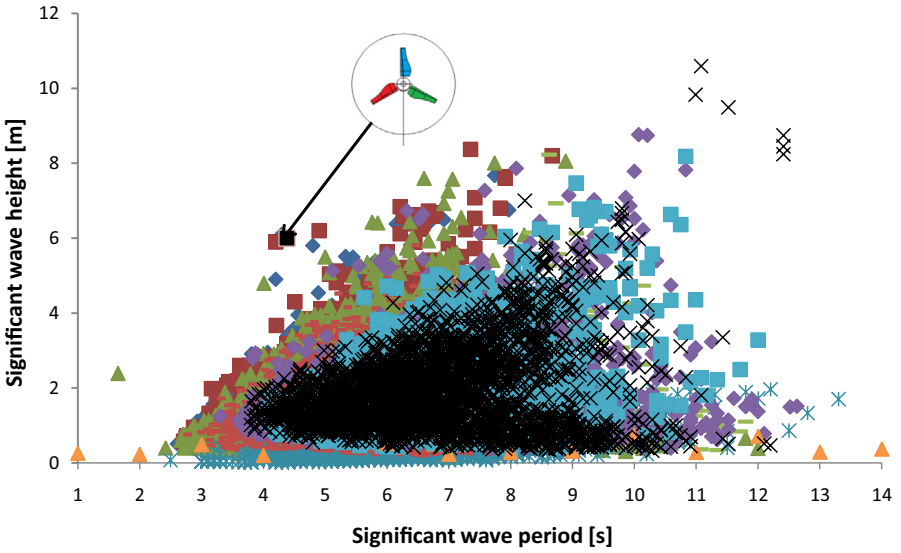

Fig. 4. Scatter plot of waves around the United Kingdom West coasts based on their significant periods and wave heights. Different colours designate different locations [22].

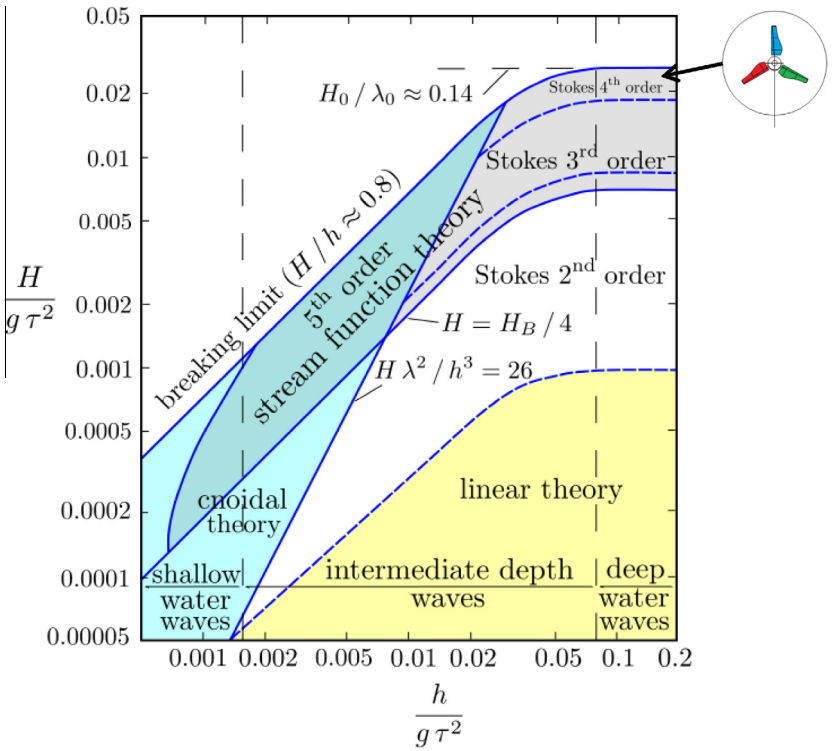

Fig. 5. Non dimensionalised water depth and wave height to determine wave regime showing the location of the wave in this study [23].

the assumption of linear theory that the amplitude of the wave is very small. Again, on Fig. 5 the wave in this study is located with the turbine symbol. A modification of linear theory was therefore applied, to account for the non-linearity of the waves due to their high amplitude of 3 m, known as Wheeler stretching [24]. This modification of linear wave theory was found to yield an approximation to the expected sub surface elliptical water motion by stretching the vertical coordinate and applying the kinematics at the mean water height throughout the water column. Further discussion of wave non-dimensionalisation and relation to the applicability of different wave theories can be found in [25] and [26].

The boundary conditions defining the height of the free surface as well as inlet conditions were specified. The fluid enters the model perpendicular to the front face at a uniform velocity of 3.086 m/s, upon which the wave and profile velocities were superimposed. The fluid exits the model through the rear face, which was set as having a downstream pressure profile due to the influence of gravity. Both of these boundaries were specified as openings, which are able to tolerate potential reverse flow in the model; a likely occurrence due to the forward and back motion of the subsurface fluid. The seabed was set as a 'No Slip' boundary to simulate the effect of the seabed and the fluid, and the side walls were specified to be 'Free Slip' to simulate a body of fluid in open sea. The top was also set as an opening to simulate the free surface.

In order to calculate the wave period from the specified wavelength of 30 m, the wave number k was first determined from Eq. (1), and then an OP wave period ω of ~4.38 s was calculated from the Dispersion Relation [26] as shown in Eq. (2).

$$L = \frac{2 \times \pi}{k} \tag{1}$$

$$\omega^2 = gk \tanh(kh) \tag{2}$$

In order to specify the linear theory in the model from the wave period k, an interpolative technique was used based on a rearrangement of Eq. (2) (and multiplication by a factor of h) and set of data pairs for (kh) and (kh tanh(kh)). This resulted in Eq. (3) in order to determine the wavenumber k given that the right hand terms are known or can be calculated. The equations for the surface elevation and subsurface water velocities could then be input directly into the boundary conditions.

$$kh \tanh(kh) = \frac{\omega^2 h}{g} \tag{3}$$

In this study, the wavelength of 30 m gave a wavenumber, k, of 0.209 m^{-1}. Given the depth of water was 35 m, the wave angular velocity was calculated as 1.43 rad/s, giving a time period of 4.38 s. The rotational speed of the turbine was once again set to 2.25 rad/s to allow direct comparison with the uncoupled CFD model. Hence a single turbine revolution takes approximately 2.79 s, thus the turbine rotates approximately 1.6 times per wave.

Once the Wheeler stretched coordinate for depth had been incorporated into the equations, the resulting horizontal subsurface velocities at different depths above the seabed are shown in Fig. 6 below. A line corresponding to the predominant flow velocity of 3.086 m/s is superimposed, and the effect of the Wheeler stretching is clearly observable as the oscillatory motion is not perfectly symmetrical around this line as would be expected with purely linear wave theory. Other differences when compared to the purely linear behaviour as shown in Fig. 7 are a slightly lower velocity due to a slight dissipation in wave amplitude, a small phase shift due to the viscous effects of the fluid in the realistic modelled case, and higher velocities near the seabed, due to the more elliptical nature of the real case as opposed to the orbital path of the mathematical case, which assumes an infinitely small amplitude as compared to the water depth. The period however is reproduced exactly as expected.

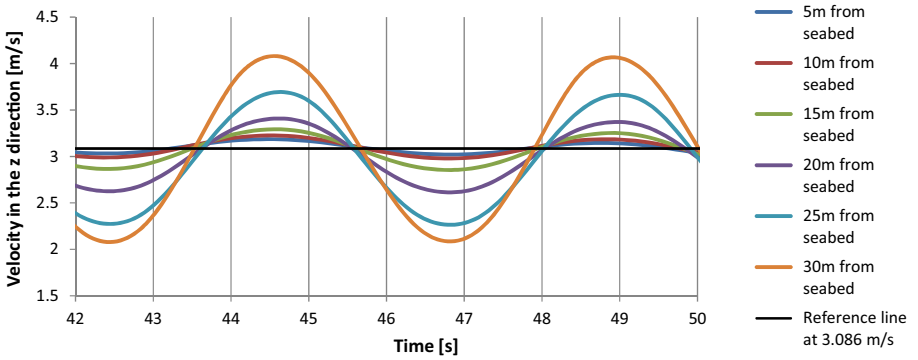

Fig. 6. Horizontal (x direction) subsurface velocities at six locations through the water column for the numerical model, incorporating Wheeler stretching.

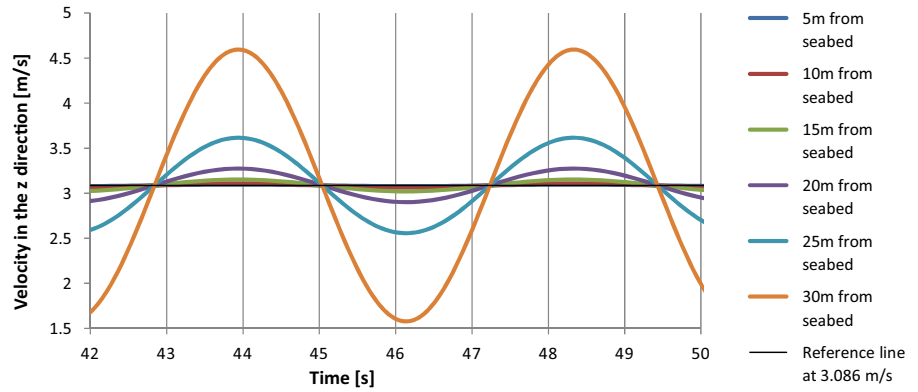

Fig. 7. Horizontal (x direction) subsurface velocities at six depths calculated using purely linear wave theory.

4. Results

4.1. Performance curves

The turbine performance characteristics were determined from the thrust and power curves plotted from the results obtained from the quasi-static model used in the uncoupled CFD analysis. Fig. 8 shows the results of both the power and thrust coefficients for the turbine with the simple support structure, which agree with previously published data that used the Reynolds Stress Model as the viscous model, i.e. peak Cp $\sim$ 0.41 at λ = 3.64 and peak Ct $\sim$ 0.80 [20,21].

Comparing the Cp and Ct values at peak power, it can be seen that when the CFD analysis is undertaken as part of the FSI model and consequently changed to a transient model, the value of both these characteristics increases. The small increase in the power output with the FSI model to 480 kW (Cp = 0.43) is partly due to deformed shape of the blades which deflect away from the non-loaded setting [9]; however as the transient FSI structural model is being compared to a very well converged steady state model, it is also possible there is some numerical error included in this, which will require some further investigation, although previous work [20] shows the minimal effect on performance parameters due to further mesh refinement. There is no significant change in the thrust with this level of blade deformation. However, as shown by Morris [9], an increasing blade deflection results in a reduction in the level of thrust, which again should be expected as the projected area reduces. This again hints towards some very small discrepancies due to the difference of model type.

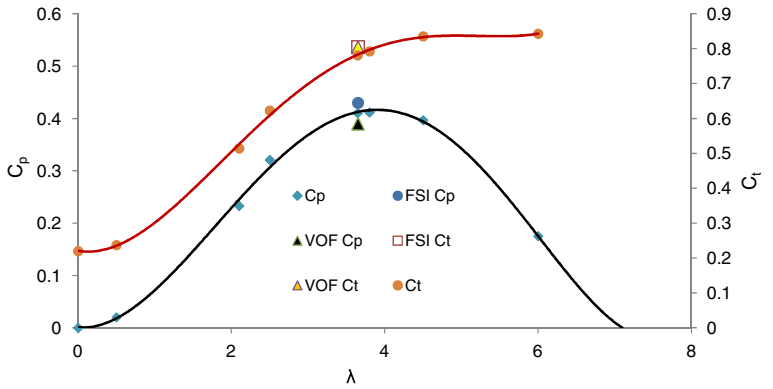

Fig. 8. Turbine performance characteristics (uncoupled CFD) with peak power and thrust values for the VOF and FSI models.

Likewise there is a similar increase in the time averaged Ct at peak power for the VOF model, though the time averaged Cp at peak power has reduced for the VOF model. From Fig. 8 it can be seen that the addition of the waves reduces the power to a mean value of approximately 440 kW (Cp = 0.38), a 4% reduction.

4.2. Thrust

Fig. 9 shows that the transient thrust force for the FSI model is reasonably constant, save for the rotational position when the blade and stanchion have a small level of interaction. The interaction per blade is once every rotation with a frequency of 0.35 Hz. Hence a complete rotation of the three bladed turbine has a frequency of 1.05 Hz. The black line is a dimensionless representation of the wave position at the turbine and the turbine images depict the blade configuration at each given time.

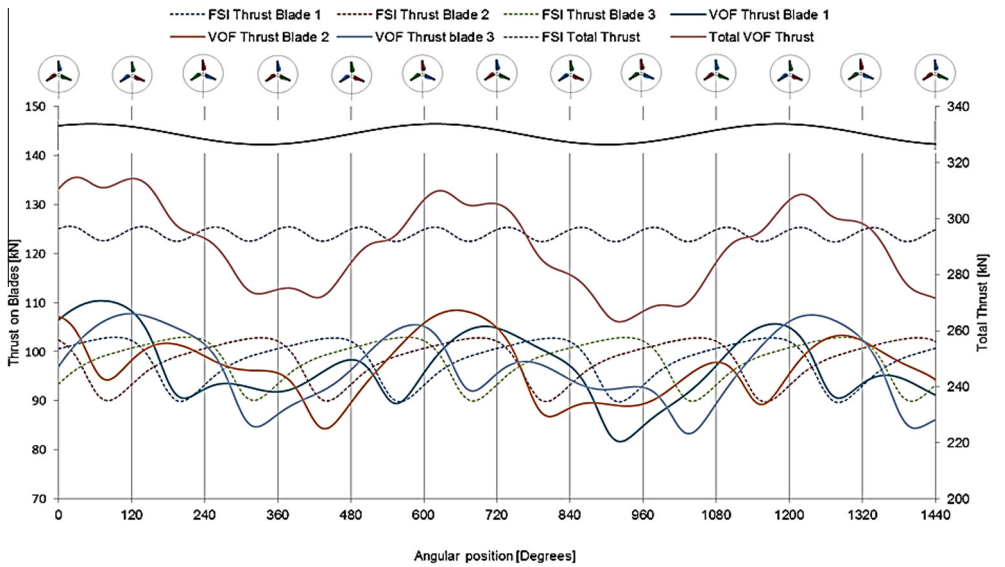

Fig. 9. Transient thrust curves for the VOF and FSI models. The top black line represents the peaks and troughs of the passing wave.

The amplitude of the thrust on an individual blade is approximately 240 kN. However the combined thrust which is transferred to the drive shaft is approximately 300 kN (Ct ~ 0.80), with a 5 kN fluctuation. This thrust and that on the hub will ultimately be transmitted to the structural support. The hub loading is negligible compared to the blade loading.

The addition of a surface wave to the environment (VOF model) can be seen to have a large effect on the thrust loading. The net thrust transferred to the drive shaft is virtually the same as that when there is no surface wave present (FSI model) as can be seen in Fig. 8. However the simple repetitive fluctuation previously seen has been complicated by the addition of a second periodic event, which has a longer time period, is not a multiple of, and out of phase of that of the turbine rotation. The maximum thrust has also increased to 318 kN (Ct ~ 0.85) with a 48 kN amplitude. However there is an additional long 'enveloping' wavelength that occurs as a result of the wave–turbine rotation combination. The frequency of this wavelength is 0.14 Hz, with amplitude of 76 kN.

4.3. Power

The power generated, with no waves present (FSI model), follows a similar trend to that of the thrust data, albeit a very slightly increased average. This is attributed to the small deflection present in the blades which have moved the blade pitch angle to the optimum value [9]. That is to say that there is a regular set of curves from each blade 120° out of phase with each other. Hence the power generated by the whole rotor is a clean repetitive power output of approximately 460 kW (i.e. Cp ~ 0.41). The frequency of the oscillation in power (approximately 12 kW) matches the rotational frequency of the turbine, i.e. 0.36 Hz. The introduction of waves reduces the power output to 450 kW (i.e. Cp ~ 0.39). The oscillation in the power, ~190 kW, has a frequency of 0.75 Hz. However there is again a longer wavelength apparent which results from the wave–turbine interaction. This influence of the waves on the turbine also means that the peak power output does not always occur at the same rotational position of the blades or with the same magnitude. From Fig. 10 it can be seen that the power peaks between one and two full rotation of the turbine for the given environment. This is in contrast to the environment with no waves, where the power peaks 3 times every full rotation of the turbine.

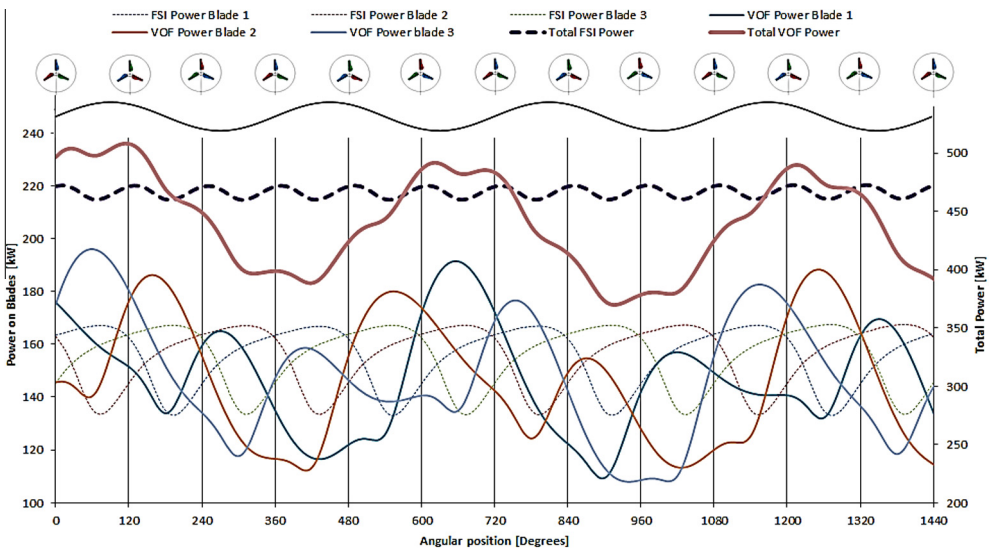

Fig. 10. Transient power curves for the VOF and FSI models. The top black line represents the peaks and troughs of the passing wave.

There is a small increase in the power output with the FSI model (Cp = 0.43, i.e. 480 kW) which can be seen in Fig. 8. This is in agreement with the findings of Morris (2014) [9], for the 3-bladed TST, who showed that the blade deflects away from the non-loaded setting and that there is a very small change in the power initially increasing as the blade deforms into an optimal position, after which point there is a drop in power output. There is no real increase in the thrust with this level of blade deformation, which is to be expected. However as shown by Morris [9] as the blades deflect the level of thrust reduces, which again should be expected as the projected area reduces.

4.4. Two way coupled FSI

Over the complete rotational cycle the blade tips deflection oscillates up to a maximum of approximately 23 mm. Since the velocity is a uniform profile this blade oscillation is induced by the presence of the stanchion. This is due to the fact that as each blade passes the stanchion its thrust and power is reduced (as represented in Figs. 8 and 9) thus causing the variation in blade deflection during a single rotation. The deflection is small relative to the length of the blades; this is due to the material properties given to the blade (steel with a Modulus of Elasticity of 200 GN/m^2) and the internal structure of the blade being solid. However, the findings are indicative of the loading distribution through the blades and hub.

Given the constantly varying loads that the blades are exposed to due to the wave and stanchion interaction as shown in Figs. 10 and 11, the blade deflections can be expected to fluctuate across a greater range of deflections in a more complex manner over a rotational cycle. Although the changes in the deflections presented here may be small there is an increased likelihood of fatigue failure and a lower life expectancy of the component parts, especially in the presence of waves. This will only be exaggerated further by a shearing flow through the water column.

4.5. Bending moments

Fig. 11 shows the resultant bending moment applied to the turbine drive shaft due to the unequal thrust loading of the tidal flow on the turbine blades. The data shown are from the VOF model and the

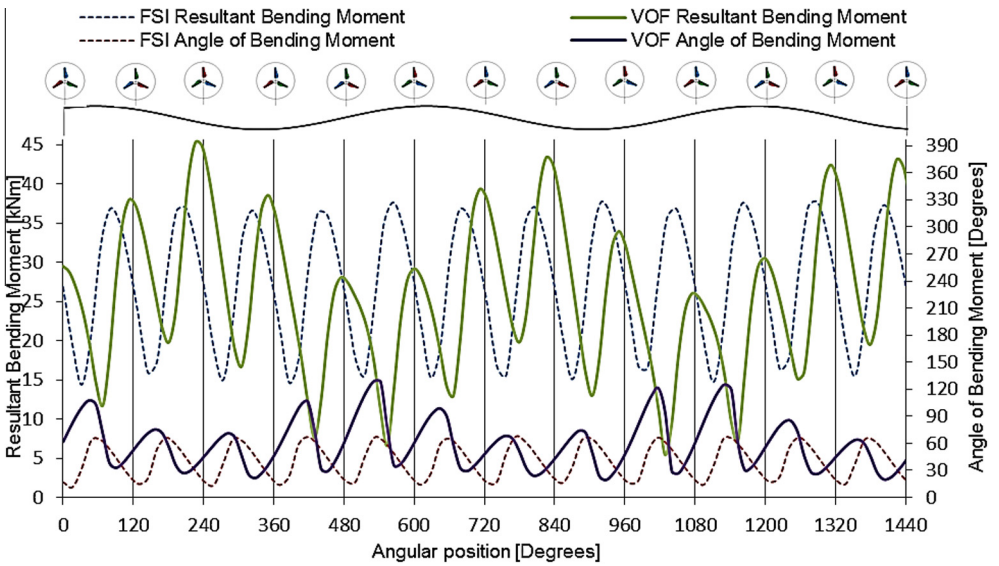

Fig. 11. Transient bending moment for the VOF and FSI model. The top black line represents the peaks and troughs of the passing wave.

FSI model respectively. The magnitudes of the bending moments are, on average, the same at 26 kN m. However, what is clear from the figure is that the FSI model, which is not influenced by waves, fluctuates between 12 and 36 kN m, whereas the introduction of waves (VOF model) increases this fluctuation to between 6 and 45 kN m.

The angle of the bending moment is defined as zero when a blade is vertically upwards at 'top dead centre' and increases in the direction of the turbine's rotation. The range of the direction of the bending moment for the FSI model is between 5° and 67°, with an average of approximately 37°. Given that the velocity is uniform the variation in angle and the fact that it remains in the upper 'quarter of the rotation' implies that the stanchion has influenced this characteristic. In contrast the introduction of the waves (VOF model) has altered the range of the bending moment direction to between 18° and 127° and the average angle to 60°. The consequence of the narrow angle range is that the bending moment will translate into loading being applied over a small area of the seals and bearings at the rotor end, resulting in uneven wear and possibly reduced life and increased maintenance requirements.

4.6. Life fatigue

Given the constantly varying loads that the blades are exposed to due to the wave interaction the corresponding deflections would also be constantly changing over a rotational cycle. Even though the changes in the deflections may be small there is an increased likelihood of fatigue failure and various failure modes. Fig. 12 highlights possible failure modes by providing an indication of the level of biaxiality. Biaxiality can be defined as 'a qualitative measure of the stress state throughout the body' [27]. This can be seen in the distribution of the stresses through the turbine rotor and nose cone. The red contours indicates pure biaxial stresses (+1), this is dominant on the nose of the hub as well as small regions at the tip of the blades and around the root of the blades on the hub. The blue contours indicate pure compressive stress (−1), this is dominant on the back of the hub and at the root of the blades. As the contours 'move' towards the zero there are areas of increasing shear stress.

Fig. 13 is a life fatigue prediction derived from the calculated strains in the structure. This is based on a fully reversible event, i.e. one cycle is considered to include flood and ebb tides. Hence if the loading history is considered to be 1.0 then the total cycles is 5.67×10^4 or 77 years. The length of this is not realistic this is partly due to the simplicity of the structural model and hydrodynamics. The

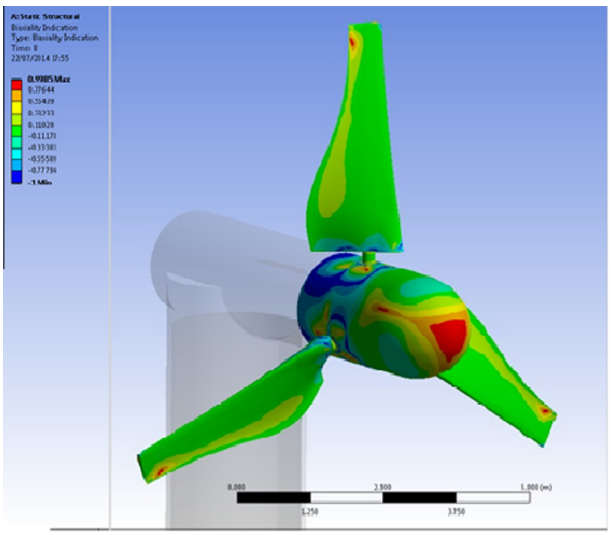

Fig. 12. Biaxial indication.

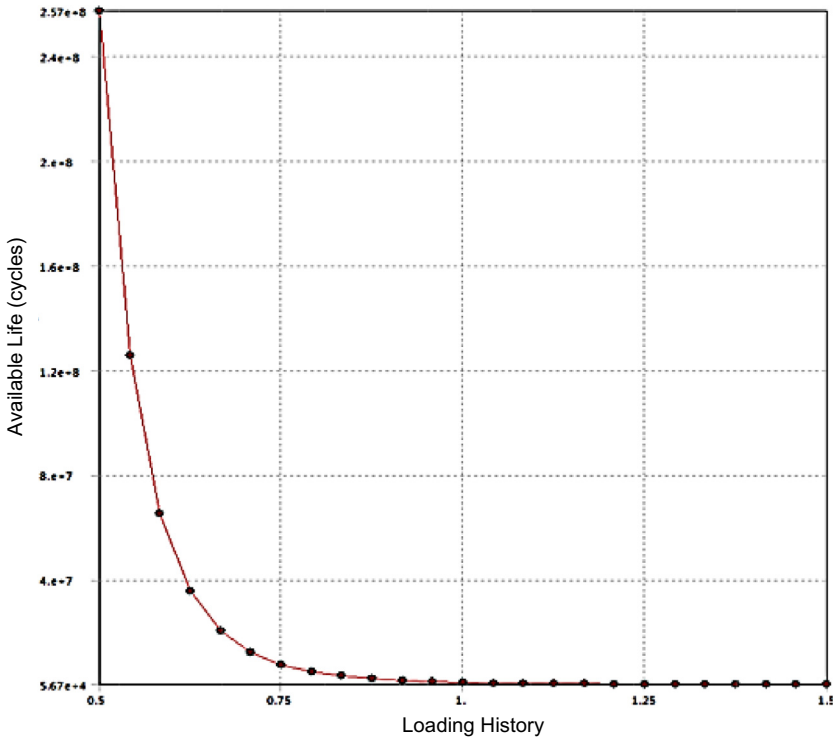

Fig. 13. Life prediction curve.

structural model consists of solid steel blades (as stated previously) with a pin connection between the blade and the hub causing a stress concentrator. These are critical components in the life prediction, and more realistic components would drastically reduce the total number of cycles. The uniform flow in both flood and ebb flows will result in an exaggerated life prediction as the true nature of the system will have complexities relating to the presence of a profiled flow and the inclusion of waves causing higher frequency and greater magnitude load cycles. The benefits of a 2 way coupled FSI model include the life prediction model and future work in this area will offer greater predictability.

4.7. Frequency analysis of loading characteristics

In order to further investigate the turbine power output and loading characteristics, under the aforementioned model conditions, frequency analysis was undertaken via the Discrete Fourier Transforms (DFT) [27,28]. The datasets produced from the CFD exercise posed limitations on the underlying frequency resolution achievable via such an analysis. This was due to the length of the data sets which were roughly 11 s of converged data. This allowed for a frequency resolution which could not be resolved into the frequency bands of interest – namely, the rotational frequency of the turbine and the frequency of the simulated wave. In order to overcome this limitation the datasets were periodised to 4 times the original datasets. This allowed for a frequency resolution of four times the original resolution thereby resolving the spectrum into the frequency bins required for the analysis.

Figs. 14 and 15 show the frequency spectrum of the axial thrust on the turbine rotor for the FSI (steady) and VOF (wave) models, respectively. The blue trace shows the thrust spectrum for a single blade whereas the red trace shows the resultant axial thrust spectrum. In both cases clear peaks are observable at the frequencies of interest, specifically at the rotational frequency of the turbine,

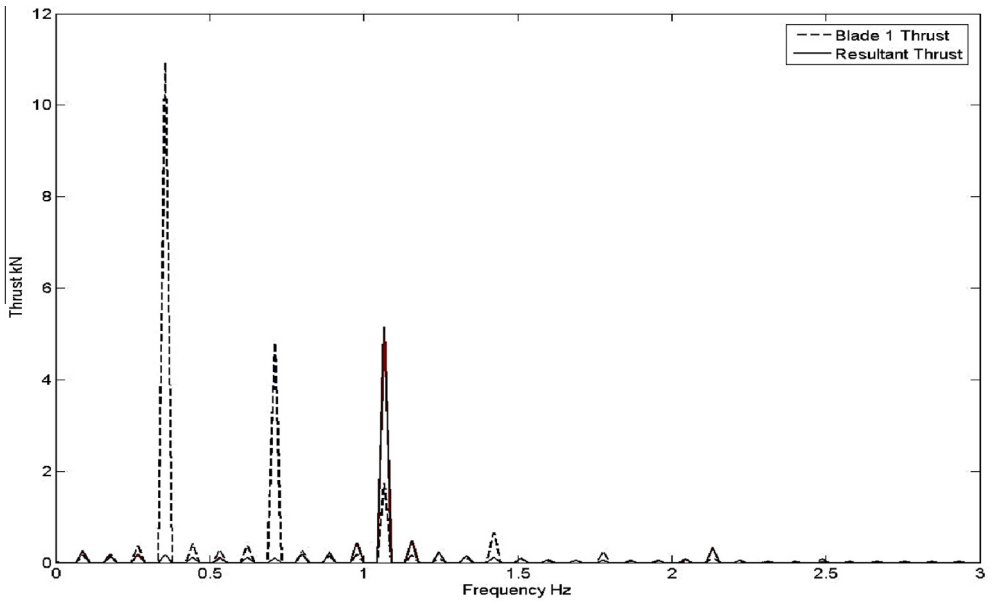

Fig. 14. Frequency spectrum for the axial thrust loading on the turbine for the FSI model showing frequency spectrum associated with a single blade (blue) and the resultant (red).

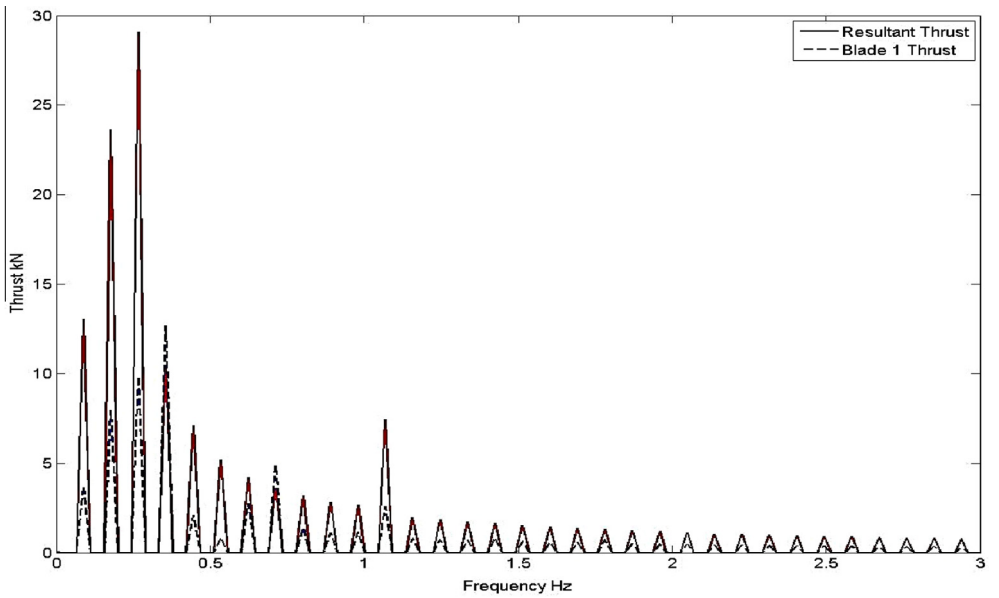

Fig. 15. Frequency spectrum for the axial thrust loading on the turbine for the VOF model showing frequency spectrum associated with a single blade (blue) and the resultant (red).

0.358 Hz (along with second, 0.717 Hz and third harmonics, 1.075 Hz) and in Fig. 15 the frequency of the wave loading is also observable.

In the case of the FSI model and steady flow conditions it can be seen, as expected, that the observed fundamental frequency is coincidental with rotational velocity of the turbine at 0.358 Hz. In the resultant case the fundamental frequency is at three times the rotational velocity of the turbine, 1.075 Hz, which is due to the interaction of the stanchion. This result can be attributed to the shift of the periodic thrust time-series due to the 120° separation of the blades. This shift in the time series for each blade leads to an associated phase shift in the frequency domain by ±120° [27]. The phase shift has resulted in deconstruction of the loading contribution from each individual blade at the rotational frequency (0.358 Hz) and twice the rotational frequency (0.717 Hz) of the turbine. This deconstruction leads to the low amplitude (approx. 0.2 kN) at the turbine rotational velocity and its 2nd harmonic in the resultant loading spectrum. Furthermore the phase shift leads to the construction of the individual blade loading characteristics at three times the rotational frequency of the turbine. Again this leads to the frequency characteristics observed in the resultant loading spectrum – specifically the 5.6 kN amplitude observed at 1.075 Hz.

Fig. 15 shows clearly that, in the VOF model data, the wave loading generates the most significant harmonic contribution to the axial thrust loading on the turbine. This is apparent in the first three peaks of the axial thrust load spectrum. The load–frequency characteristics associated with the wave are distributed over three frequency bands. The bands consist of two lower frequency components at 0.089 Hz and 0.178 Hz with the third and most significant peak at 0.267 Hz, which is approximately equal to the wave frequency. The thrust loading fluctuations associated with the turbine rotation can also be observed, albeit with less significance in terms of the overall load spectrum. The constructive and destructive interference observed in the FSI model data, due to the associated phase shifting, has been disrupted by the presence of the simulated wave. This resulted in higher load fluctuations at the rotational frequency of the turbine (0.358 Hz) in the resultant load spectrum. The effect of the wave load has, over the lower frequency ranges, resulted in a more complex spectrum with more disparate loading frequencies. This scenario, in reality, could be far more varied and complex given the wave spectra observed under realistic sea conditions.

5. Discussion

The exact placement of a tidal turbine in the water column will be dependent on a number of issues. These issues include the design of the anchoring method, the seabed topography, the shipping needs, the environmental considerations, etc. What must be known is the velocity profile over a period of time including spring and neap tides, the approximate level of turbulence and a history of the wave characteristics. With this information not only can the device characteristics be determined, but also the extreme loadings under normal conditions. The fundamental effects of how the waves change the velocity of the water through the water column can be estimated from oceanographic texts, such as [23] and [26]. However, the effects of these changes on a turbine are another matter.

The work discussed in this paper has shown that as expected the average thrust on the turbine and power generated are only affected by a small amount. It is interesting to note that the average thrust has a small increase of approximately 5%, whilst the average power is reduced by approximately 5%.

Galloway et al. [13] found that there was no change in the average power and thrust due to the addition of waves, which in an idealised set up would be expected due to the symmetrical back and forth motion of the wave velocities. However, their experiment was conducted in a towing tank, with no real interaction of the waves and current, whereas this study was purely numerical, allowing interaction between the two and the frictional effect of the seabed. They state in their paper that real wave current interaction is more complex and prone to error and lack of understanding. This more complex environment could account for this discrepancy. In addition, there is no experimental error in the numerical model, just a very minimal residual calculation error, whereas the Galloway study was subject to experimental error and vibrational effects from the towing infrastructure. However, they found the cyclic variation was significant, with a 37% variation in thrust, and 35% variation in power, values which are dependent on the wave. Similar conclusions were drawn by Lust et al. [14]

and Luznik et al. [15], but again, these experiments took place in a towing tank, limiting the interaction between waves and currents. For their wave they found an 18% cyclic increase in power and a 35% cyclic minimum in power. The study in this modelling paper was for a wave out of phase with the turbine, so the peaks and troughs of the wave coincided with different turbine positions. In addition, the wave was more extreme than those mentioned in the previous papers, so had a greater effect on the turbine. Therefore a further factor is that if the model were run for a much longer time, it is expected that the variation in average power and thrust would be reduced as all combinations of wave and turbine position would be achieved.

Therefore the major problems arise from the large increase in the fluctuations in these characteristics. It should be noted that the turbine was run at a constant rotational speed and with a fixed blade pitch angle, facts that would not be true in reality and that one or both could be varied in response to fluctuations. The structure's response time to wave induced velocity changes would still produce large fluctuations as the inertia effects of the rotor would play a significant role. The fluctuations will translate into increased wear and tear or fatigue on components of the turbine, so reducing the life expectancy of the device before maintenance would be required. The amplitude of the fluctuations is most likely related to the wavelength and celerity of the wave and would have to be designed for. It could be hypothesised that the waves cause low frequency fatigue, with turbulence causing high frequency fatigue under certain circumstances. This work has not included an ADCP derived velocity profile and wave combined. However, it can be further hypothesised that given the possibility of a high shear velocity profile through the water column and the increased loading amplitude the results discussed in this paper will only be exaggerated under such conditions.

The FSI model has provided an insight into the reaction of the turbine, specifically the blades, to the simple uniform velocity. Due to the material chosen for the blades, the deflections are relatively small at approximately 23 mm, however there is a minor interaction with the structure as the blades pass in front of the stanchion. There are clearly fluctuations in the loading on the individual blades that cause a fluctuation in the deflection of the blades as it rotates. These fluctuations cause a 'pulsing' in the thrust transferred to the drive shaft, as well as a resultant bending moment. The consequences are likely to be a reduced life expectancy before maintenance would be required. If the results of a wave were superimposed onto the loads then the blade roots and drive shaft will be subjected to large fluctuations in loads and bending moments.

The frequency content of the loading and power output from the turbine, under both the wave and plug flow conditions, suggests that coincidence of the turbine rotational velocity with the wave frequency could lead to greater load and power fluctuations as well as increased peak loading. This could be significant for extreme load predictions and would require that turbine developers survey the wave climate at prospective development sights. This surveying process should then be carried out with the goal of observing the correlation between frequencies observed in the given wave climate and the expected rotational velocity range of the turbine. The finding also adds to the need for intelligent turbine control schemes to minimise wave load fluctuation. To further explore this notion further modelling of wave climates would be required. The more complex frequency characteristic in the wave loading case suggest that fatigue life predictions will be dependent on the wave climate at proposed turbine deployment sites and as such could be a function of a complex wave spectra. However, it is likely that the effect of the wave spectra will be band limited due to the limited depth of penetration of higher frequency waves.

6. Conclusions

This paper has discussed the influence of waves on a tidal turbine's characteristics. What is clear is that the waves change the time averaged values of power and thrust. However the magnitudes and period of the changes are most likely dependent on the wave definition, i.e. wavelength, amplitude and celerity.

The amplitude of the fluctuations in both the power and thrust become exaggerated with waves as the axial flow velocity is influenced by the wave's subsurface rotational component.

There is clearly a need to include waves in the modelling of marine devices provided the devices are within a water column depth, to the surface, of half the wavelength of a wave.

The results from the two-way coupled FSI models have shown no significant differences from those of the uncoupled CFD model. However, this phenomenon is not a construct of weak fluid structure coupling but is primarily a result of the unrealistic inflexibility of the blade material at that scale and will therefore require further investigation. This latter point is especially true with the introduction of waves as presented in this paper.

The frequency analysis has shown that the wave frequency creates a more complex thrust load spectra. The interaction of wave frequency and turbine rotational velocity should be considered both in terms of potential deployment sight surveying and turbine control.

Acknowledgements

The authors would like to express their gratitude for the support of EPSRC – United Kingdom, WEFO LCRI Marine, HPC Wales, Fujitsu (UK), and Mabey Bridge Ltd – United Kingdom for their funding of the work. The support of ANSYS is also gratefully acknowledged.

References

[1] European Union Committee, 27th Report of Session 2007–08 – The EU's Target for Renewable Energy: 20% by 2020, The Stationery Office Limited, London, 2008.
[2] DECC, UK Renewable Energy Roadmap Update 2012 Crown copyright, Dept of Energy & Climate Change, London, 2012.
[3] Carbon Trust, Accelerating marine energy: the potential for cost reduction: insights from the carbon trust marine energy accelerator, 2011.
[4] de Laleu V, La Rance Tidal Power Plant. 40-year operation feedback – lessons learnt, in: BHA Annual conference. <www.british-hydro.org/downloads/La%20Rance-BHA-Oct%202009.pdf>, 2009 (accessed July 2014).
[5] Tidal Energy Limited, <www.tidalenergyltd.com> (accessed July 2014).
[6] Seagen Wales, <http://seagenwales.co.uk/description.php> (accessed July 2014).
[7] Royal Haskoning, SeaGen Environmental Monitoring Programme Final Report [Online]. Available at: <http://www.marineturbines.com/sites/default/files/SeaGen-Environmental-Monitoring-Programme-Final-Report.pdf>, 2011 (accessed 2 March 2013).
[8] A. Mason-Jones, P.S. Evans, T. O'Doherty, D.M. O'Doherty, Characterisation of a tidal stream turbine design using CFD and ADCP, in: World Renewable Energy Conference, Glasgow, 2008.
[9] C.E. Morris, Influence of solidity on the performance, swirl characteristics, wake recovery and blade deflection of a horizontal axis tidal turbine (Ph.D. thesis), Cardiff University, 2014. <http://orca.cf.ac.uk/60952>.
[10] P.R. Pinet, Invitation to Oceanography, fifth ed., Jones & Bartlett Publishers, 2009. p. 237. ISBN 0-7637-5993-3.
[11] M. Lewis, S.P. Neill, M.R. Hashemi, Waves, wave direction and the tidal stream energy resource, in: TOS/ASLO/AGU Ocean Sciences meeting, 23–28 February 2014, Honolulu, Hawaii, 2014, <http://www.eposters.net/pdfs/waves-wave-direction-and-the-tidal-stream-energy-resource.pdf> (accessed July 2014).
[12] L.E. Myers, A.S. Bahaj, An experimental investigation simulating flow effects in first generation marine current energy converter arrays, Renewable Energy 37 (2012) 28–36.
[13] P.J. Galloway, L.E. Myers, A.S. Bahaj, Studies of a scale tidal turbine in close proximity to waves, in: 3rd International Conference on Ocean Energy, 6 October 2010, Bilbao, 2010.
[14] E.E. Lust, L. Luznik, K.A. Flack, J.M. Walker, M.C. Van Benthem, The influence of surface gravity waves on marine current turbine performance, Int. J. Mar. Energy 3 (4) (2013) 27–40.
[15] L. Luznik, K.A. Flack, E.E. Lust, K. Taylor, The effect of surface waves on the performance characteristics of a model tidal turbine, Renewable Energy 58 (2013) 108–114.
[16] R.F. Nicholls-Lee, S.R. Turnock, S.W. Boyd, A method for analysing FSI on a HATT, in: 9th European Wave and Tidal Energy Conference. Southampton, 5–9 September 2011, 2011.
[17] S.W. Park, S. Park, S.H. Rhee, Performance predictions of a horizontal axis tidal stream turbine considering the effects of blade deformation, in: 3rd International Symposium on Marine Propulsors, Launceston, 5–8 May 2013, 2013.
[18] A. Mason-Jones, D.M. O'Doherty, C.E. Morris, T. O'Doherty, Influence of a velocity profile & support structure on tidal stream turbine performance, Renewable Energy (2012), http://dx.doi.org/10.1016/j.renene.2012.10.022.
[19] C. Frost, C.E Morris, A. Mason-Jones, D.M. O'Doherty, T. O'Doherty, Effects of tidal directionality on tidal turbine characteristics, J. Renewable Energy (2015), http://dx.doi.org/10.1016/j.renene.2015.01.053.
[20] A. Mason-Jones, D.M. O'Doherty, C.E. Morris, T. O'Doherty, C.B. Byrne, P.W. Prickett, R.I. Grosvenor, I. Owen, S. Tedds, R.J. Poole, Non-dimensional scaling of tidal stream turbines, Energy (2012), http://dx.doi.org/10.1016/j.energy.2012.05.0102012.
[21] S.C. Tedds, R.J. Poole, I. Owen, G. Najafian, A. Mason-Jones, C.E. Morris, T. O'Doherty, D.M. O'Doherty, Experimental investigation of horizontal axis tidal stream turbines, in: 9th EWTEC, Southampton , 2011.
[22] British Oceanographic Data Centre, Wave Data Series for Cardigan Bay, Port Talbot, The Mumbles, Gower and the Severn Estuary, British Oceanographic Data Centre, Liverpool, 2013.
[23] B. Méhauté, An Introduction to Hydrodynamics and Water Waves, Springer-Verlag, New York, 1976.

[24] J.D. Wheeler, Method for calculating forces produced by irregular waves, in: Preprints 1969 Offshore Technology Conference, 1(1007), 1969, pp. 83–94.
[25] American Petroleum Institute, Recommended Practice for Planning, Designing and Constructing Fixed [20] Offshore Platforms API-RP2A, 21st ed., API, Washington, DC, USA, 2000;
United States Army Corps of Engineers, Shore Protection Manual, Department of the Army, Mississippi, USA, 1984.
[26] J. Pedlosky, Waves in the Ocean and Atmosphere – Introduction to Wave Dynamics, Springer-Verlag, New York, 2003.
[27] A.V. Oppenheim, A.S. Willsky, S.H. Nawab, Signals & Systems, Prentice Hall, Upper Saddle River, NJ, 1997.
[28] S.W. Smith, The Scientist and Engineer's Guide to Digital Signal Processing, first ed., California Technical Pub, San Diego, Calif., 1997.